Rapid #: -13100915

CROSS REF ID: **646339**

LENDER: **UPM :: Ejournals**

BORROWER: **MFM :: Main Library**

TYPE:	Article CC:CCG
JOURNAL TITLE:	Magazine of Concrete Research
USER JOURNAL TITLE:	Magazine of Concrete Research
ARTICLE TITLE:	Influence of curing regime and steel fibres on the mechanical properties of UHPC
ARTICLE AUTHOR:	
VOLUME:	67
ISSUE:	18
MONTH:	September
YEAR:	2015
PAGES:	988 - 1002
ISSN:	0024-9831
OCLC #:	

Processed by RapidX: 4/3/2018 6:31:30 AM

Magazine of Concrete Research
Volume 67 Issue 18

Influence of curing regime and steel fibres on the mechanical properties of UHPC
Prem, Ramachandra Murthy and Bharatkumar

Magazine of Concrete Research, 2015, **67**(18), 988–1002
http://dx.doi.org/10.1680/macr.14.00333
Paper 1400333
Received 10/10/2014; revised 18/12/2014; accepted 22/12/2014
Published online ahead of print 28/02/2015

ice
Institution of Civil Engineers
publishing

Influence of curing regime and steel fibres on the mechanical properties of UHPC

Prabhat Ranjan Prem
Scientist, CSIR Structural Engineering Research Centre, Chennai, India
Avadhanam Ramachandra Murthy
Senior Scientist, CSIR Structural Engineering Research Centre, Chennai, India
Bhajantri H. Bharatkumar
Senior Principal Scientist, CSIR Structural Engineering Research Centre, Chennai, India

The effect of accelerated curing and steel fibre volume on ultra-high performance concrete (UHPC) is the focus of this paper. The compressive strength and microstructural properties of UHPC were evaluated under water, steam and heat curing. The results show that heat-cured samples have higher mechanical properties than those undergoing the other curing techniques. Experimental studies were conducted on heat-treated specimens with different steel fibre volumes and aspect ratios (2·5% and 2·0% of 13 mm and 6 mm length fibres of diameter 0·16 mm) to examine stress–strain behaviour, tensile behaviour and flexure behaviour. The stress–strain behaviour of UHPC was evaluated by uniaxial compression tests on cylinders to propose a new stress–strain model for UHPC under compression. Size-dependent and size-independent fracture energies were determined as per the Rilem procedure and the *P–δ* tail correction method. Flexural and residual strengths were evaluated under four-point bending.

Notation

a_0	crack length
d	diameter of steel fibre
$E_{c,u}$	secant modulus
E_{if}	initial tangent modulus of steel-fibre-reinforced concrete
E_{inf}	slope at inflection point
E_{it}	initial tangent modulus of normal concrete
E_o	tangent modulus of elasticity at the origin
f_{ck}	compressive stress
f'_{cf}	compressive strength of fibre concrete
G_f	fracture energy
l	length of steel fibres
P	applied load
r	correlation coefficient
t	specimen thickness
V_f	volume fraction of steel fibres
W	specimen depth
W_F	work of fracture
w	crack mouth opening displacement
β	material parameter
ε_c	strain
$\varepsilon_{c,u}$	peak strain
ε_o	strain at peak stress
σ	stress
$\sigma_{c,u}$	peak stress

Introduction

Studies have recently been conducted to examine the fracture properties of high-strength and ultra-high-strength concrete beams under the size effect (Ramachandra Murthy *et al.*, 2013a). Further size-independent specific fracture energies of concrete mixes have been determined by two methods and a trilinear model (Karihaloo *et al.*, 2013; Ramachandra Murthy *et al.*, 2013b, 2013c). The effect of curing and fibre volume on the mechanical properties of the ultra-high-performance concrete (UHPC) is extended in this study by examining the compressive, tensile and flexural properties.

In the present research, UHPC is concrete of compressive strength greater than 150 MPa. Its constituents were cement, fine sand, silica fume, quartz powder, superplasticiser (SP), a low water/cement ratio and high-strength micro steel fibres (BFUP AFGC, 2002). The literature reveals that the observed compressive strength of UHPC samples is dependent on the hydration of cement, pozzolanic reactions of silica fume at lower temperatures and the combined action of silica fume and quartz at higher temperatures (Zheng *et al.*, 2014). Accelerated curing is needed for proper development of the microstructure of calcium silicate hydrates (Ambily *et al.*, 2013; Cheyrezy *et al.*, 1995; Habel *et al.*, 2006; Prem *et al.*, 2013; Wille *et al.*, 2012). To examine the effect of curing on UHPC samples, compression tests and microstructural studies were carried out on specimens cured with water, steam and heat. Based on these results, experiments were conducted to study the effect of fibre volume on heat-treated specimens.

Studies on the compressive properties of UHPC have been conducted but the effect of reinforcement index (RI) on the stress–strain behaviour of UHPC under uniaxial compression has not been reported (Graybeal, 2007; Tayeh *et al.*, 2012). The work described here evaluated the stress–strain characteristics of UHPC

with different steel fibre volumes under uniaxial compression. Empirical relationships between various parameters of the stress–strain curve were evaluated to propose a stress–strain model for UHPC in compression and the proposed model is compared and assessed with existing models from the literature. Tensile behaviour was evaluated by conducting split tensile tests and three-point bending tests on notched specimens. The load against crack mouth opening displacement (CMOD) obtained from three-point bending tests was used to evaluate fracture energy. The flexural performance of UHPC was measured using the test method ASTM C1609/C1609M-05 (ASTM, 2006).

Materials and methods

Mix design

The UHPC mix design is given in Table 1. The silica fume/cement ratio and quartz powder/cement ratio were 0·25 and 0·40 respectively. Sand was used as a filler and SP was added to the mix to improve workability (Karihaloo *et al.*, 2013; Ramachandra Murthy *et al.*, 2013a, 2013b, 2013c; Prem *et al.*, 2013). Five batches of UHPC were cast with varying fibre volumes (called R1, R2, R3, R4 and R5). The density of the mixtures was in the range 2460–2520 kg/m^3. Mix R2 was used to identify the ideal curing regime.

Material properties

Ordinary Portland cement (grade 53, conforming to Indian standard IS 12269:1987) (BIS, 1987) was used. According to IS 4031, the tested 28 d cement compressive strength was 58 MPa. The specific gravity was 3·15 and the initial and final setting times were 110 min and 260 min respectively. The normal consistency was 28% and the particle size range was 31–7·5 μm.

The silica fume used in the experiment conformed to ASTM C1240 (ASTM, 2014). Its specific gravity was 2·25, the percentage passing through a 45 μm sieve in wet sieve analysis was 92% and the particle size range was 5·3–1·8 μm.

The quartz powder used had a specific gravity of 2·59. The percentage passing through a 45 μm sieve in wet sieve analysis was 75% and the particle size range was 5·3–1·3 μm.

Two types of sand were used: grade I (coarse, particle size range 0·60–2·36 mm) and grade III (fine, particle size range 0·075–0·150 mm). A polyacrylic ester based type SP was also used. The tensile strength of the steel fibres was 2000 MPa.

Mixing

A planetary mixer of 300 kg capacity was used to cast the UHPC. The advantage of this mixer is its simultaneous rotation of the mixing drum and the blades, hence providing uniform blending of the materials. Mixing was carried out at three speeds – low, medium and high – each for 10 min. At slow speed, dry binder powder was poured into the pan and mixed. Around 30% of the water–SP mixture was then added at medium speed. At high speed, 50% of the water and SP was added to inhibit homogeneity in the mix. Steel fibres was added to the mix manually through an open split at the top of the drum, and finally the remaining 20% of the SP and water were added and the drum was rotated at very high speed for 10 min.

Curing

For water curing, after demoulding, the samples were kept in water until the date of testing (i.e. after 3, 7, 14 and 28 d). For steam curing, demoulded samples were subjected to a curing temperature of 100°C and relative humidity of 95% for 18 h in a steam curing chamber. The delay period was 2 h and the rate of temperature rise was 20–30°C/h, thus taking around 4 h to reach peak temperature. After 18 h, the samples were removed from the curing chamber and allowed to attain thermal equilibrium with the atmosphere (another 4 h); they were then kept in water until the day of testing. An ultrathermal cyclic chamber was used for heat curing, for which the temperature can rise up to +300°C ± 1°C. The rate of rise and drop in temperature is 2°C/minute. Before being subjected to heat curing, the samples were kept in water and then exposed to a temperature of 200°C for 48 h from the third day, after which they were allowed to attain thermal equilibrium with the atmosphere and then kept in water until testing (Graybeal and Hartmann, 2003; Prem *et al.*, 2013; Yazıcı *et al.*, 2009).

Casting and testing

Curing studies were conducted on mix R2, for which 36 cubes of dimensions 70 mm × 70 mm × 70 mm were cast. Compression

Mix	Cement: kg/m^3	Silica fume: kg/m^3	Quartz powder: kg/m^3	Fine aggregate: kg/m^3	Water: l/m^3	SP: l/m^3	Steel fibres		RI	w/c ratio
							Type [a]	Vol: %		
R1	788	197	315	866·8	173	14·77	SF1	2·5	2·0312	0·22
R2	788	197	315	866·8	173	14·77	SF1	2·0	1·6250	0·22
R3	788	197	315	866·8	173	14·77	SF2	2·5	0·9375	0·22
R4	788	197	315	866·8	173	14·77	SF2	2·0	0·7500	0·22
R5	788	197	315	866·8	173	14·77	—	—	0·0000	0·22

[a] SF1, 13 mm length and 0·16 mm diameter; SF2, 6 mm length and 0·16 mm diameter

Table 1. Composition of UHPC mixes R1, R2, R3, R4 and R5

testing was carried out on cube specimens under water-saturated surface dry condition, after 3, 7, 14 and 28 d as per ASTM C1609 (ASTM, 2006). The tests were performed in a 3000 kN capacity compression testing machine with load applied at the rate of 0·2 kN/s. Powder obtained from the crushed cubes after testing were taken for X-ray diffraction (XRD) analysis.

To determine the stress–strain characteristics of mixes R1–R5 in compression, uniaxial compression tests were carried out on concrete cylinder specimens of size 100 × 200 mm. Linear variable differential transformers (LVDTs) and strain gauges were instrumented on the cylinder and readings were finalised by taking the average values of five cylinders for each mix. The readings were recorded by an HBM datalogger connected to the control system. The tested cylinders were kept in cross-head control with a constant deformation rate of 0·2 mm/min until peak load and 0·05 mm/min for the post-peak stage. The test was continued until the load dropped to more than 50% of peak load or until failure. The compressive strengths of mixes R1–R5 (size 100 mm × 100 mm × 100 mm) were tested at 7, 14, 21 and 28 d. Testing was carried out as per ASTM C1609 (ASTM, 2006) and the final reading taken was the average of four cubes.

The tensile behaviour of mixes R1–R5 was determined by testing simply supported notched beam specimens under three-point loading and split tensile strength. Centre-loaded notched concrete beams were tested under a closed-loop servo-controlled compression testing machine of capacity 3000 kN, with the rate of opening being 0·0005 mm/s. The CMOD was measured by a clip gauge attached with knife edges epoxied to the bottom flange on either side of the starter notch. An LVDT was rigidly fastened to the reference frame with the moving tips lying on a plate fastened to one of the two halves of the specimen. The tests were carried out on beams of size 70 mm × 70 mm × 350 mm for mixes R1–R5. The notch-to-depth ratio of the beam specimens was 0·3 and the clear span was 300 mm. The deflection observed from the beam and the clip gauge could be compared using the datalogger connected to the control.

The flexural performance of mixes R1–R5 was measured using the test method ASTM C1609 (ASTM, 2006). The beams used were 70 mm × 70 mm × 350 mm with a clear span of 300 mm. Deflection was measured from an LVDT attached to the frame and the load signal was measured from a load cell directly attached to the bottom of the cross-head. A 5 Hz data acquisition frequency was used to record static load and deflection signals. The final reading was taken as the average of three prisms.

Results and discussion

Curing

The compressive strengths of cubes cured with normal, steam and heat curing are listed in Table 2. The samples thermally cured for 2 d and then water cured showed the highest strength results at all ages. At the age of 7 d, steam curing and heat curing produced better results (120 MPa and 160 MPa respectively) than water curing (64 MPa). The strength results vary widely among the techniques, but the highest strength was always achieved with heat curing. At 14 d and 28 d there was not much difference between water curing and steam curing. This is because only high early-age strength is achieved with steam curing: the strength at later ages is the same as for standard curing (Husem and Gozutok, 2005; Liu *et al.*, 2005).

Age at testing: d	Compressive strength: MPa		
	Water curing	Steam curing	Heat curing
3	53	53	53
7	64	120	160
14	111	128	185
28	144	142	196

Table 2. Compressive strength of cubes

The thermal regime is highly significant for curing UHPC in order to activate silica fume and quartz powder: if not applied, the materials will act only as filler materials and not as binders. The chemical reaction of binders develops simultaneously in an interdependent way, resulting in a solid skeleton progressive formation and rearrangement of hydration products, which are responsible for strength development.

The diffractograms of 28 d water curing, steam curing and heat curing are shown in Figures 1, 2 and 3 respectively. With all the three curing regimes, the 28 d XRD results indicate the formation of quartz peaks in abundance, which can be due to the presence of silica fume and quartz powder in the mix. Also, calcite, tobermorite and tricalcium silicates are also present to some extent. The diffractogram of 28 d heat curing shown in Figure 3 indicates compound formation similar to that of the other two curing regimes, but the difference lies in the intensity and additional quartz peak formation as shown in the circled areas of the diffractogram between the 2θ values of 30–36° and 50–75°. Also, the formation of portlandite within the 2θ values of 30–36° and the formation of tricalcium alumino ferrite (brownmillerite) within the 2θ values of 50–75° is seen only in the heat curing diffractogram shown in Figure 3, which can be due to increased rate of hydration owing to high thermal regime, responsible for the highest compressive strength of 196 MPa.

Based on the curing results, heat treatment was adopted for further investigations.

Compressive behaviour

Compressive strength

The compressive strengths of heat-treated mixes R1–R5 evaluated at 7, 14, 21 and 28 d are shown Table 3, which shows that the

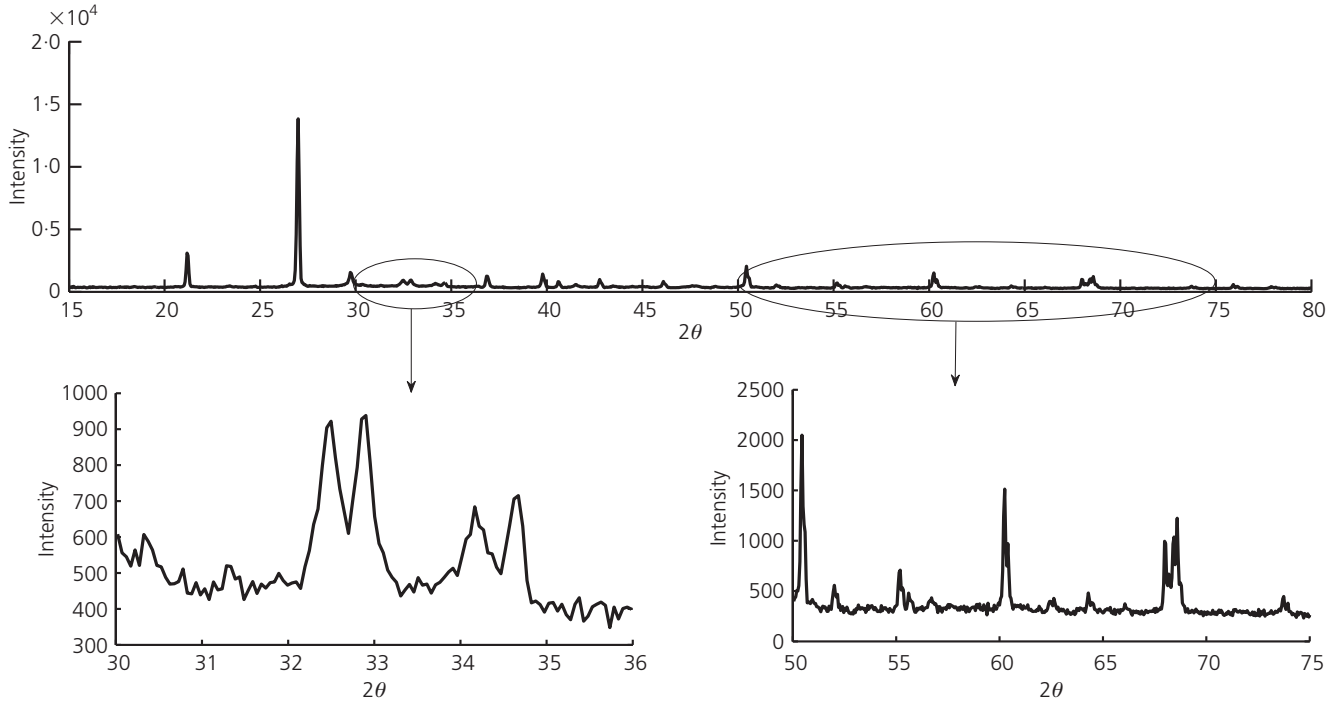

Figure 1. XRD analysis for water curing

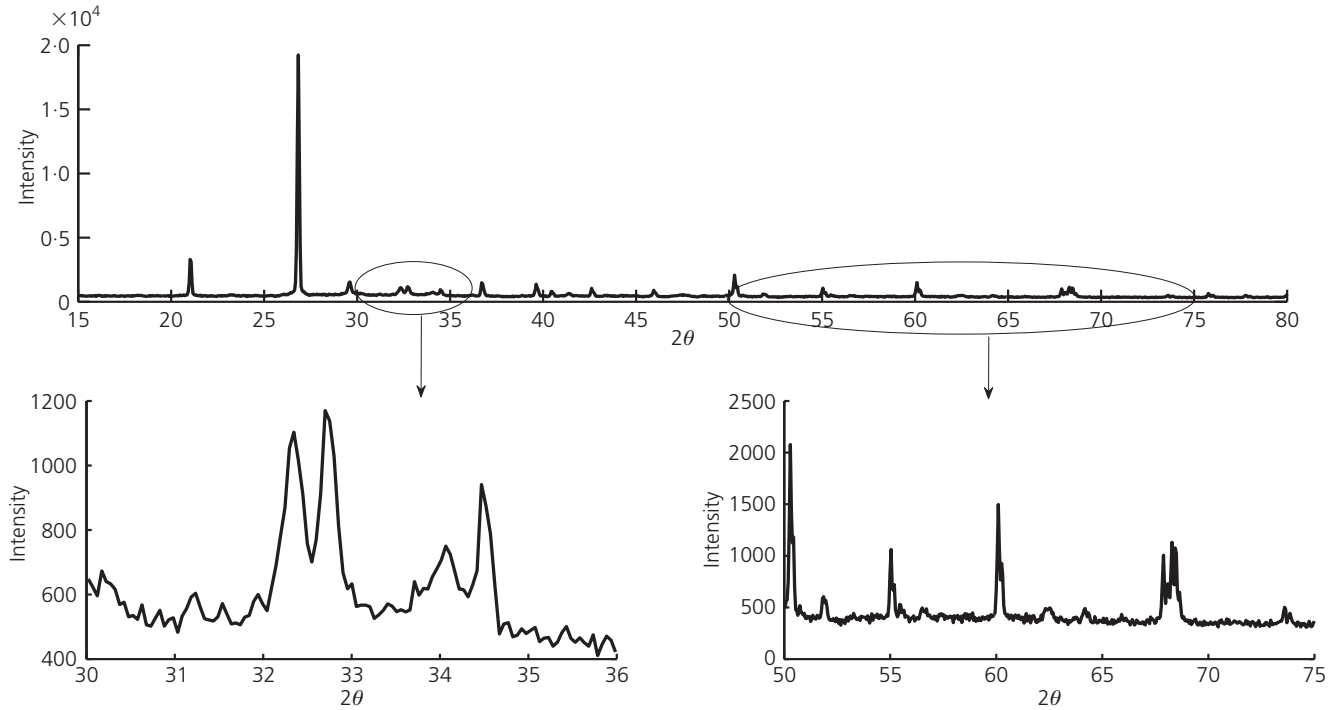

Figure 2. XRD analysis for steam curing

specimens attained 90% of their compressive strength at the age of 14 d. Mixes having the same fibre volume irrespective of aspect ratio produced a 25% increment in compressive strength compared with that of the control mix.

Similar compressive strengths were observed for mixes R1, R3 and R2, R4 at the age of 28 d. The highest strength was recorded for R1 (180·28 MPa). These results indicate that the incorporation of micro steel fibres at similar volumes gave similar compressive

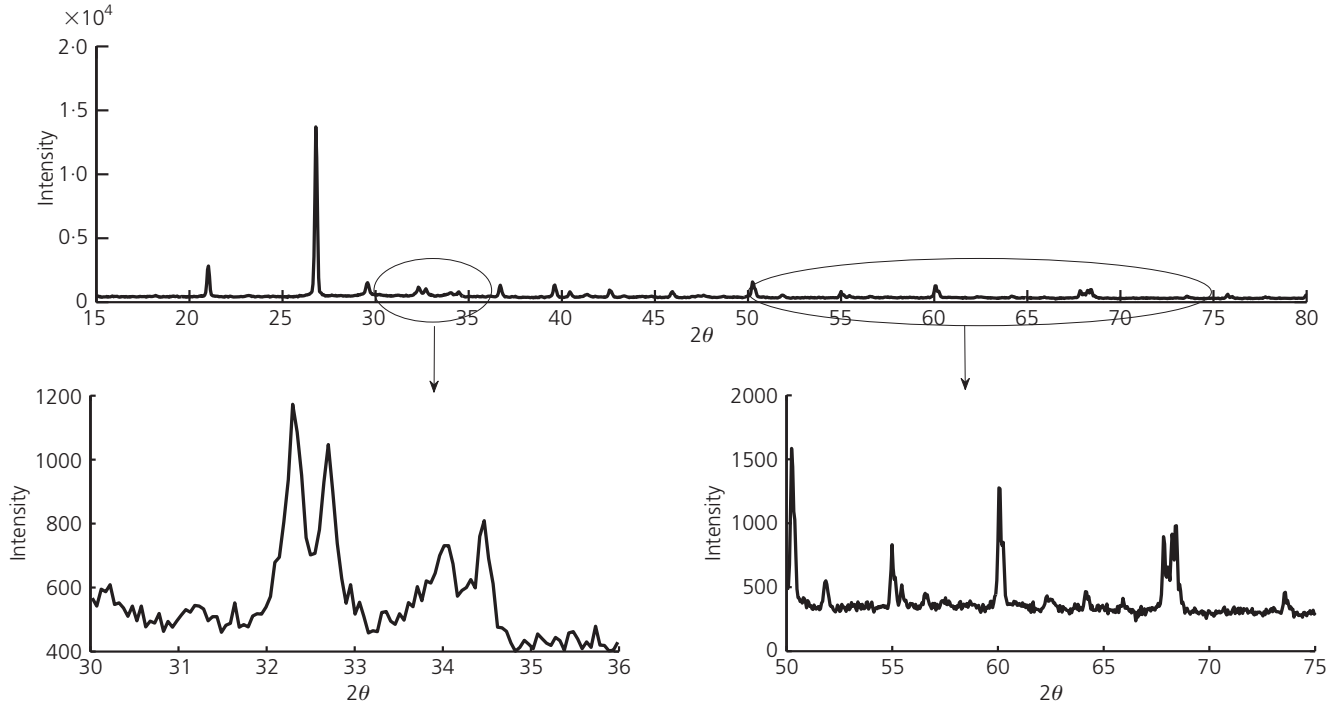

Figure 3. XRD analysis for heat curing

Mix	Compressive strength: N/mm^2			
	7 d	14 d	21 d	28 d
R1	152·67	168·5	176·4	180·28
R2	147·20	162·3	167·3	170·29
R3	149·50	167·2	172·0	178·70
R4	129·80	149·7	156·0	164·00
R5	104·00	123·0	126·0	132·00

Table 3. Cube strength evaluated at 7, 14, 21 and 28 d for R1, R2, R3, R4 and R5

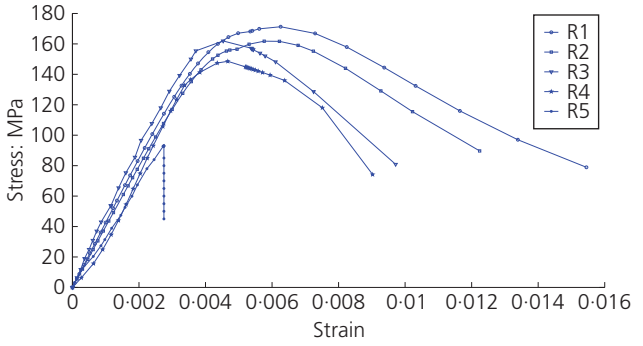

Figure 4. Stress–strain behaviour of mixes R1–R5

strengths irrespective of the aspect ratio (in this case 40 and 81). The lowest strength was obtained for mix R5 (132 MPa), with no steel fibres.

Stress–strain behaviour

The stress–strain response was recorded by uniaxial loading on cylinders and is shown in Figure 4. The stress–strain characteristics show that pre-peak regions have a linear ascending portion and the strain at peak stress increases with an increase in strength and RI. The post-peak curve is strongly dependent on the fibre type and fibre content and it is almost as steep as the ascending curve for lower fibre contents and may be more gradually sloping for the higher fibre contents.

The failure patterns of tested cylinders (Figure 5) showed that mixes R1 and R2, having long fibres, failed mostly due to the formation of multiple cracks, with failure in the principal diagonal direction. Mixes R3 and R4, having short fibres, failed due to the formation of vertical cracks, with more localised failure. Crushing of specimens made from R3 and R4 was more significant than for R1 and R2 specimens. It is noted that multiple cracking leads to higher failure strain and the redistribution of stresses leads to higher residual strength.

Very limited studies to develop a stress–strain model for UHPC have been carried out. A model to predict the empirical relationships of UHPC under uniaxial compression is proposed next.

Figure 5. Failure patterns of cylinder specimens of mixes R1–R5

Theoretical modelling

Several studies have been reported in the literature for predicting the stress–strain behaviour of normal-strength and high-strength concrete (Aslani and Nejadi, 2013; Hognestad, 1951; Popovics, 1973; Wee *et al.*, 1996). The stress (σ) in any of these concrete models depends on the tangent modulus of elasticity at the origin (E_o), the strain (ε_c) value at that corresponding point, peak stress ($\sigma_{c,u}$) and peak strain ($\varepsilon_{c,u}$). The post-peak behaviour of the concrete is incorporated by considering the secant modulus ($E_{c,u}$) at the peak (Yip, 1998). With the development of fibre-reinforced concrete (FRC) (Balaguru and Shah, 1992; Zollo, 1997), the strain capacity and deflection hardening of concrete mixes have increased considerably. Steel fibres, which form the basic component of fibre concrete, increase post-ductility, toughness, flexural strength, fatigue strength, tensile strength and cause specimens to fail by micro cracking.

Bhargava *et al.* (2006), Ezeldin and Balaguru (1992), Nataraja *et al.* (1999) and Ou *et al.* (2011) proposed analytical expressions for generating the stress–strain curve of FRC based on the expression proposed by Carreira and Chu (1985) for uniaxial compression of plain concrete. Review of the models reveals that the area under the stress–strain curve increases with respect to both volume fraction and aspect ratio (l/d). A common parameter, known as the reinforcement index ($\mathrm{RI} = V_f \times l/d$ in which V_f, l and d are the volume fraction, length and diameter of steel fibres in the mix respectively), combines the effect of fibre volume and aspect ratio. A material parameter (β), which is dimensionless, needs to be evaluated from the physical properties of the stress–strain curve (Bhargava *et al.*, 2006; Carreira and Chu, 1985; Ezeldin and Balaguru, 1992; Nataraja *et al.*, 1999; Ou *et al.*, 2011). In the present study, experimental work was carried out to study the stress–strain behaviour of UHPC. The model of Carreira and Chu (1985) is used as a basis to obtain constitutive relations for UHPC. Details of the existing models are now given.

CARREIRA AND CHU (1985) MODEL

The model proposed by Carreira and Chu (1985) for unconfined plain concrete is a general form of a serpentine curve represented by Equations 1 and 2.

$$1.\quad \frac{\sigma}{\sigma_{c,u}} = \frac{\beta(\varepsilon_c/\varepsilon_{c,u})}{\beta - 1 + (\varepsilon_c/\varepsilon_{c,u})^{\beta}}$$

$$2.\quad \beta = \frac{1}{1 - (\sigma_{c,u}/\varepsilon_{c,u}E_{it})}$$

EZELDIN AND BALAGURU (1992) MODEL

Compression tests on cylindrical steel-fibre-reinforced concrete (SFRC) specimens with hooked-end steel fibres with compressive strength 35–85 MPa were carried out. Three fibre volume fractions of (30, 45 and 60 kg/m^3) and three aspect ratios (60, 75 and 100) were investigated. The RI ranged from 0·23 to 0·77. The relationships obtained are

$$3.\quad \sigma_{c,u}\ (\mathrm{MPa}) = \sigma + 3{\cdot}51(\mathrm{RI}) \qquad r = 0{\cdot}75$$

$$4.\quad \varepsilon_{c,u} = \varepsilon_o + 446 \times 10^{-6}(\mathrm{RI}) \qquad r = 0{\cdot}70$$

$$5.\quad \beta = 1{\cdot}093 + 0{\cdot}7132(\mathrm{RI})^{-0{\cdot}926}$$

$$\text{RI} = V_f \frac{l}{d} \quad (6)$$

in which RI is the reinforcement index calculated on the basis of the volume fraction of fibres and ε_o is suggested to be 0·002.

NATARAJA *ET AL.* (1999) MODEL

Nataraja *et al.* (1999) used crimped fibres in their study to generate a complete stress–strain curve for SFRC of compressive strength 30–50 MPa. Three volume fractions (0·50%, 0·75% and 1·00%; 39, 59 and 78 kg/m^3) and two aspect ratios (55 and 82) were considered. The RI ranged from 0·28 to 0·82. The proposed model is given by

$$\sigma_{c,u}(\text{MPa}) = \sigma + 2{\cdot}1604(\text{RI}) \quad (7)$$
$$r = 0{\cdot}76, \; f_{ck} < 50 \text{ MPa}$$

$$\varepsilon_{c,u} = \varepsilon_o + 0{\cdot}0006(\text{RI}) \qquad r = 0{\cdot}94 \quad (8)$$

$$\beta = 0{\cdot}5811 + 1{\cdot}93(\text{RI})^{-0{\cdot}7406} \qquad r = 0{\cdot}96 \quad (9)$$

$$E_{inf} = 1930(\text{RI})^{-0{\cdot}7406} \qquad r = 0{\cdot}97 \quad (10)$$

BHARGAVA *ET AL.* (2006) MODEL

The model of Bhargava *et al.* (2006) proposes stress–strain curves for concrete of compressive strength 58–76 MPa. The volume fractions ranged from 0·5% to 2·0% and two aspect ratios were considered (20 and 40). The equations take into account the effect of mixing long fibres and short fibres by considering reinforcement indices of short fibres $(\text{RI})_s$ and long fibres $(\text{RI})_L$. The relationships assume constants k_1 and k_2 to be 1 for the ascending portion. The formulations for stress–strain response are given by Equations 11– 21.

$$\frac{\sigma}{\sigma_{c,u}} = \frac{k_1\beta(\varepsilon_c/\varepsilon_{c,u})}{k_1\beta - 1 + (\varepsilon_c/\varepsilon_{c,u})^{k_2\beta}} \quad (11)$$

E_{if} = initial tangent modulus of SFRC (12)

E_{it} = initial tangent modulus of normal concrete (13)

$$\beta = \left(\frac{\sigma_{c,u}}{A}\right)^3 + C \quad (14)$$

$$A = 50{\cdot}35 + 22{\cdot}31(\text{RI})_s + 19{\cdot}31(\text{RI})_L \quad (15)$$

$$C = 2{\cdot}04 - 0{\cdot}313(\text{RI})_s - 0{\cdot}155(\text{RI})_L \quad (16)$$

For the ascending portion $k_1 = k_2 = 1$

$$k_1 = \left(\frac{D}{\sigma_{c,u}}\right)^{3{\cdot}79} \quad (17a)$$

$$k_2 = \left(\frac{G}{\sigma_{c,u}}\right)^{1{\cdot}46} \quad (17b)$$

$$D = 35{\cdot}635 + 17{\cdot}21(\text{RI})_s + 9{\cdot}11(\text{RI})_L \quad (18a)$$

$$G = 31{\cdot}82 + 16{\cdot}39(\text{RI})_s + 9{\cdot}35(\text{RI})_L \quad (18b)$$

$$\sigma_{c,u} = \sigma + 0{\cdot}45 + 8{\cdot}89(\text{RI})_s + 2{\cdot}47(\text{RI})_L \quad (19)$$

$$\varepsilon_{c,u} = \varepsilon_o - 0{\cdot}00026 + 0{\cdot}001214(\text{RI})_s + 0{\cdot}00086(\text{RI})_L \quad (20)$$

$$E_{if} = E_{it} + 422 - 603(\text{RI})_s - 597(\text{RI})_L \quad (21)$$

OU *ET AL.* (2011) MODEL

The model was developed for the compressive stress–strain curve of SFRC for values of RI up to 1·7. It is observed that the descending branch of the stress–strain curve becomes less steep as RI increases. However, as RI increases from 1·3 to 1·7, the descending branch varies insignificantly. The model predicts a slightly steeper descending branch for RI = 1·7 than for RI = 1·3. The empirical relationships are given by Equations 22–25

$$\sigma_{c,u}(\text{MPa}) = \sigma + 2{\cdot}35(\text{RI}) \quad (22)$$

23. $\varepsilon_{c,u} = \varepsilon_o + 0{\cdot}0007(\mathrm{RI})$

24. $\beta = 0{\cdot}71(\mathrm{RI})^2 - 2{\cdot}0(\mathrm{RI}) + 3{\cdot}05$

25. $\text{Toughness index} = -0{\cdot}54(\mathrm{RI})^2 + 1{\cdot}90(\mathrm{RI}) + 0{\cdot}88$

PROPOSED MODEL

Physical parameters such as toughness ratio, toughness index, modulus of elasticity and β obtained from the experimental results are compared with the RI in Figures 6–9. Toughness is a measure of the ability to absorb energy during deformation. In this work, toughness was estimated using the area under the stress–strain curves until the strain of 0·0154, which is five times the ultimate concrete strain of 0·003 adopted in the ACI code requirements for structural concrete (ACI 318-08; ACI (2008)). Ezeldin and Balaguru (1992) and Nataraja *et al.* (1999) used this strain to represent the post-peak behaviour. The toughness ratio and toughness index are given by

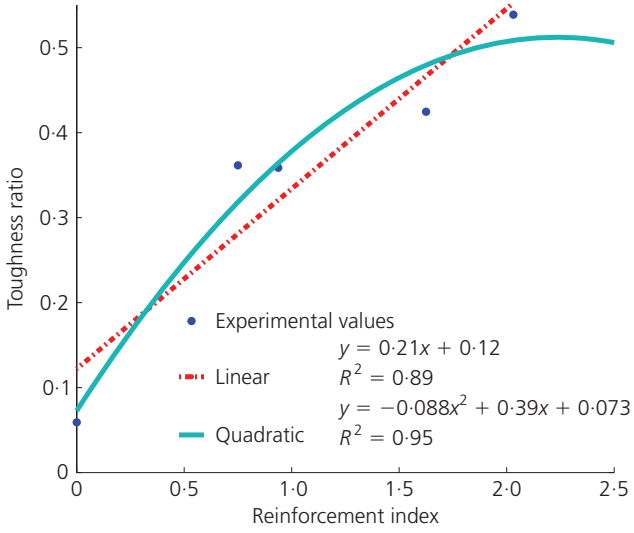

Figure 6. Toughness ratio plotted against reinforcement index

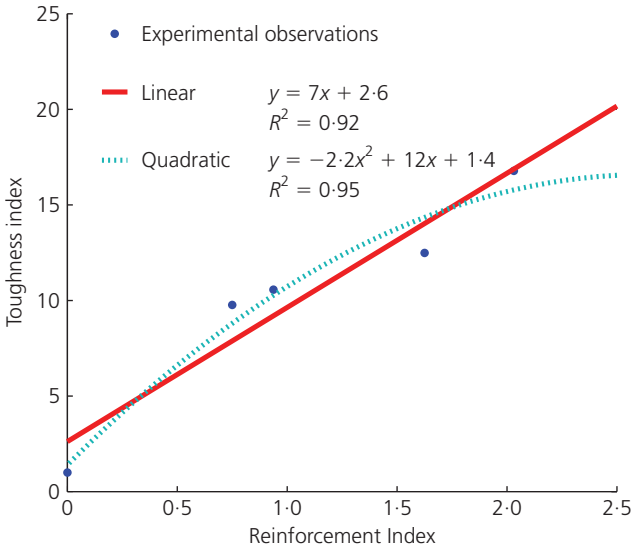

Figure 7. Toughness index plotted against reinforcement index

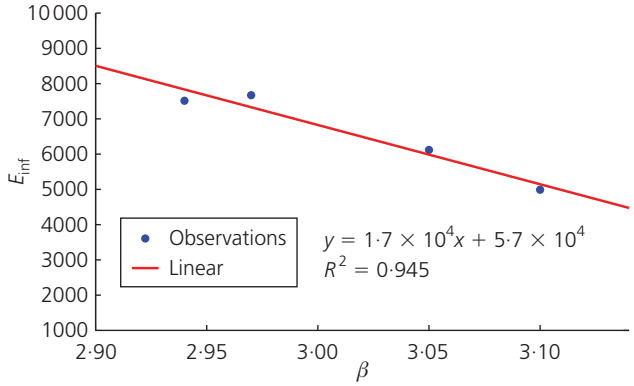

Figure 8. E_{inf} plotted against β

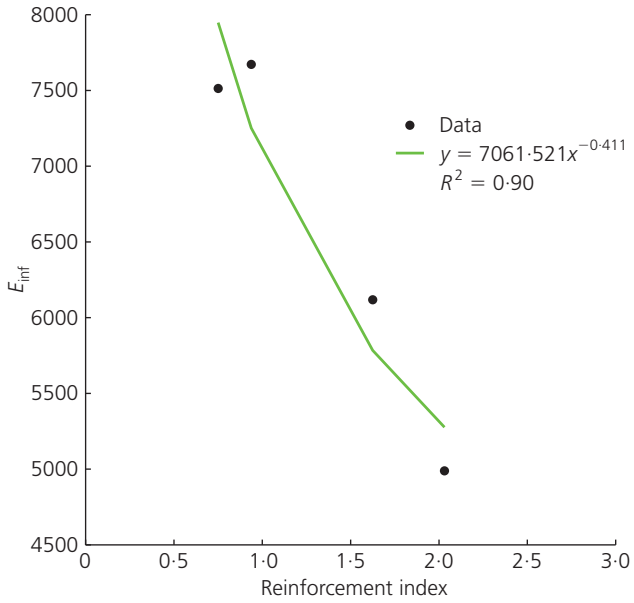

Figure 9. Elastic modulus (inflection point) plotted against reinforcement index

26. $\text{Toughness ratio} = \dfrac{ED}{0{\cdot}015 f'_{cf}}$

27. $\text{Toughness index} = \dfrac{ED}{ED_c}$

in which ED is the energy absorption capacity of concrete with fibres or the area under the stress–strain curve until strain of 0·0154 and ED_c is the energy absorption capacity of the control specimen defined up to a strain of 0·0154. It is observed in the present work that the peak strain increases with an increase in RI. On performing regression analysis shown in Figures 6–9, it was found that the toughness ratio and toughness index show a very good correlation with the RI. It is also noted that fibres play a crucial role in the compressive stress–strain curve in the descending branch. From the experimental results, a best-fit statistical analysis was performed to obtain a relationship between E_{inf}, β and RI. E_{inf} is calculated by evaluating the slope at the inflection point of the descending segment obtained from the stress–strain curve (Nataraja *et al.*, 1999). This slope, represented by E_{inf}, shows the behaviour of concrete in the post-peak region. Regression analysis reveals that the elastic modulus and secant modulus have a very weak correlation with the RI. For higher fibre contents and longer fibre length, larger values of toughness ratio and toughness index are obtained, indicating the effective contribution of steel fibres to concrete toughness.

The following model (Equations 28–32) is proposed for UHPC

$$E_{inf} = -16805\beta + 57241 \quad R^2 = 0{\cdot}9455 \tag{28}$$

$$E_{inf} = 7061{\cdot}5(\mathrm{RI}) - 0{\cdot}411 \quad R^2 = 0{\cdot}90 \tag{29}$$

$$\beta = 3{\cdot}406 + 0{\cdot}420(\mathrm{RI})^{-0.411} \tag{30}$$

$$\text{Toughness ratio} = -0{\cdot}088(\mathrm{RI})^2 + 0{\cdot}3934(\mathrm{RI}) + 0{\cdot}0727 \quad R^2 = 0{\cdot}9522 \tag{31}$$

$$\text{Toughness index} = -2{\cdot}181(\mathrm{RI})^2 + 11{\cdot}515(\mathrm{RI}) + 1{\cdot}394 \quad R^2 = 0{\cdot}958 \tag{32}$$

With the help of the proposed model, β can be found from knowledge of the RI. The stress–strain response of UHPC mixes R1–R4 was taken as the input value and compared with existing models (Bhargava *et al.*, 2006; Carreira and Chu, 1985; Ezeldin and Balaguru, 1992; Nataraja *et al.*, 1999; Ou *et al.*, 2011). Figures 10–13 show the assessment of models for R1–R4 respectively. Mix R5 showed brittle failure, due to which there was a sudden drop for the post-peak region. Hence the behaviour consists of only the pre-peak region, which matched the proposed model and most of the existing models well. The models of Ezeldin and Balaguru and Nataraja *et al.* overestimate the pre-peak region and underestimate the post-peak region. The Bhargava *et al.* model assumes two separate constants for the stress–strain behaviour and is not able to predict the behaviour for all mixes R1–R4. The post-peak behaviour showed a very sudden fall; the parameters given by this model fit SFRC but need to be refined for UHPC. The model of Ou *et al.* predicts the ascending portion but this model again overestimates stress values in the post-peak region. The proposed model is for RI in the range 0·0 to 2·0. The model satisfactorily fits the experimental results.

Tensile behaviour

Split tensile strength

The results of split tensile tests conducted on the cylinders are shown in Table 4. The results show that there is good enhancement in tensile strength upon the addition of steel fibres. The

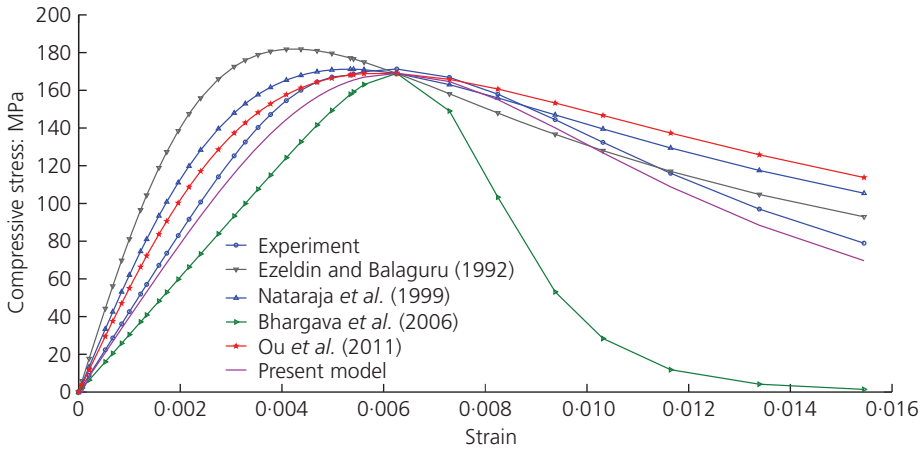

Figure 10. Comparison of concrete models for mix R1

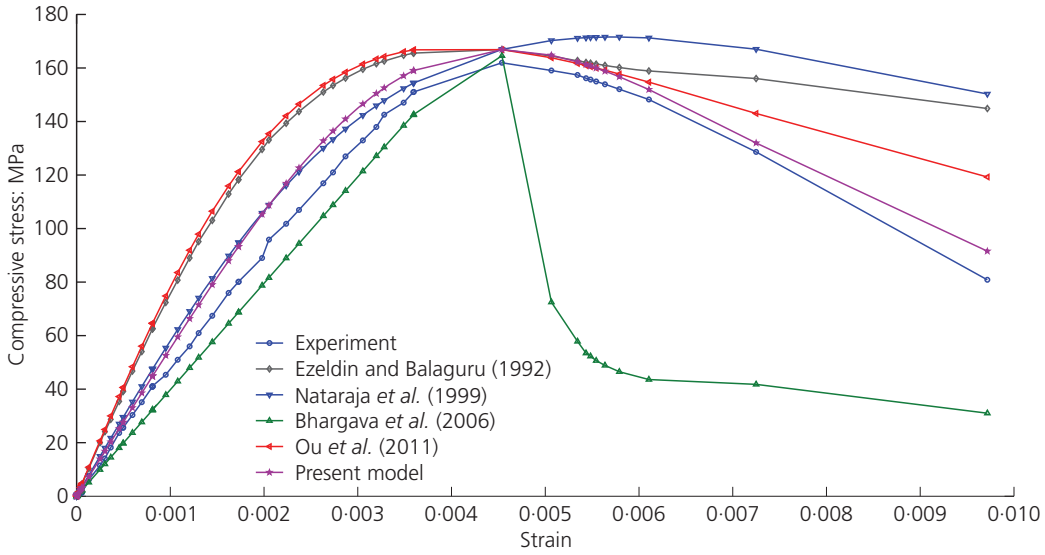

Figure 11. Comparison of concrete models for mix R2

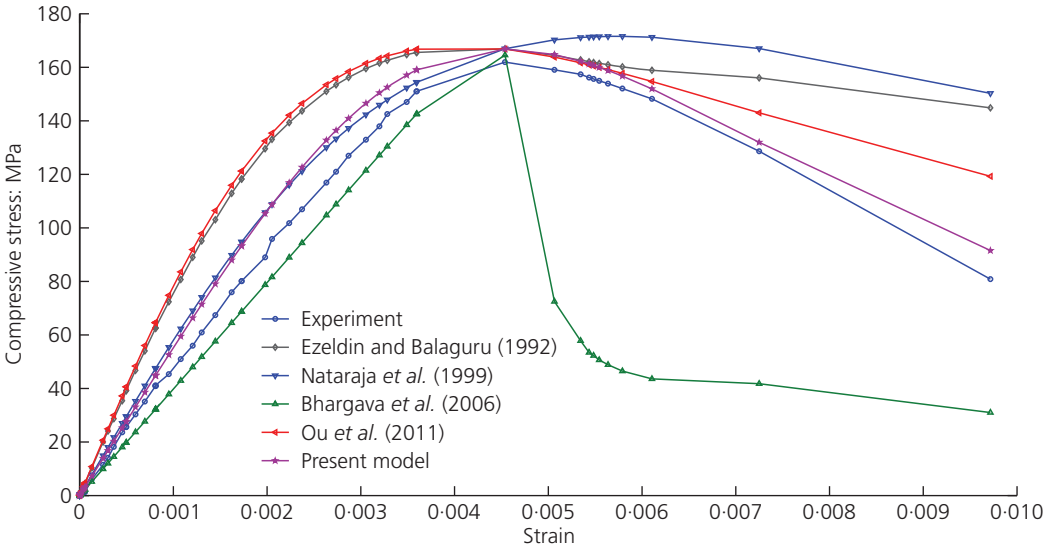

Figure 12. Comparison of concrete models for mix R3

addition of small fibres produced a lower tensile strength than the addition of long fibres. The results indicate that the size-dependent fracture energy and toughness of the mixes are in the order R1 > R2 > R3 > R4 > R5.

Size-dependent fracture energy

The tensile fracture behaviour of quasi-brittle materials can be evaluated by the fracture energy G_f (Wittmann *et al.*, 1990), which is defined as the amount of energy necessary to create a crack of unit surface area projected in a plane parallel to the crack direction. The area under the load–displacement plot is considered the work of fracture (W_F), defined as

$$W_F(w) = \int_0^w P \, dw \quad (33)$$

where w is the CMOD and P is the applied load. According to the Rilem method (Vandewalle, 2000) adopted from Hillerborg *et al.* (1976), the fracture energy G_f is the average energy given by dividing the total work of fracture by the projected fracture area. In the case of a specimen of depth W, initial crack length a_0 and thickness t, the fracture energy is given by

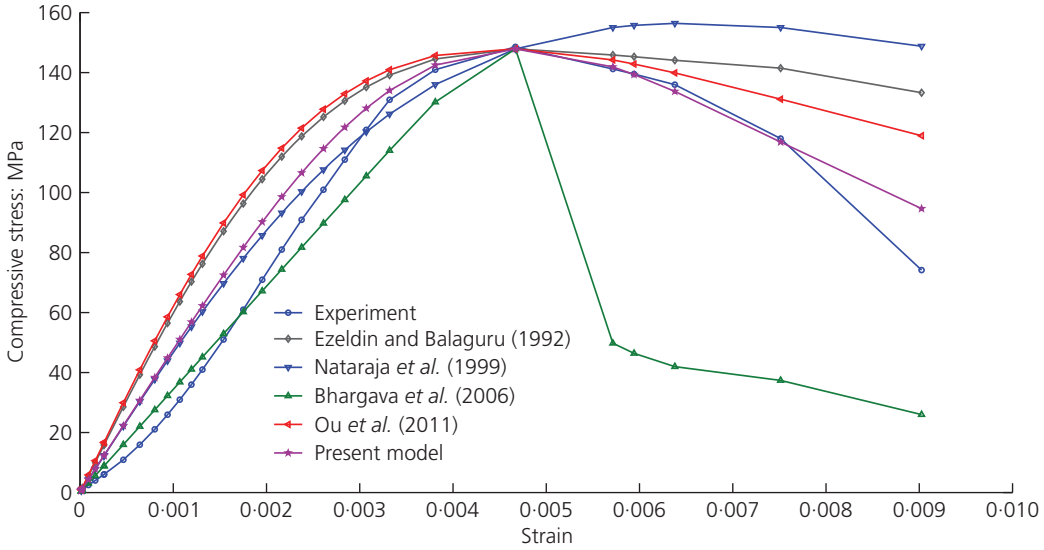

Figure 13. Comparison of concrete models for mix R4

Mix	Split tensile strength: N/mm^2
R1	23·8
R2	22·6
R3	20·2
R4	18·0
R5	11·3

Table 4. Split tensile strength evaluated at 28 d for R1, R2, R3, R4 and R5

$$G_f = \frac{W_F}{(W - a_0)t} \quad (34)$$

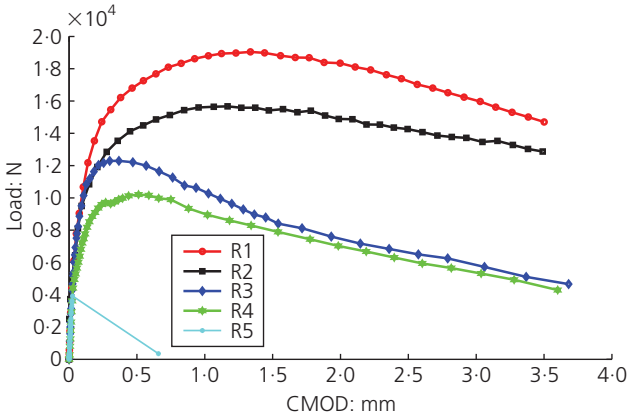

Figure 14. Load plotted against crack mouth opening displacement

The size-dependent fracture energy was obtained for mixes R1–R5 using the Rilem work of fracture method (Rilem 50-FMC, 1985). The load–CMOD of mixes R1–R5 were obtained according to the Rilem TC 162 recommendations (Vandewalle, 2000). The CMOD was measured up to 3·5–4·0 mm due to limitations of the clip gauge, as shown in Figure 14. The mix with longer fibres had a much higher bridging action, meaning that these beams had a very high resistance to cracking. The mix with smaller fibres had a more descending type of curve. The control mix R5, however, showed brittle failure. Table 5 shows the size-dependent fracture energy for mixes R1–R5: the fracture energy and toughness of the mix are in the order R1 > R2 > R3 > R4 > R5.

Mix	Size-dependent fracture energy, G_f: N/m	Size-independent fracture energy by P–δ tail correction: N/m
R1	17 512	33 214
R2	14 323	33 085
R3	8474	11 020
R4	7516	9768
R5	422	422

Table 5. Size-dependent and size-independent fracture energy for mixes R1–R5

Size-independent fracture energy

From the literature (Ramachandra Murthy *et al.*, 2013b) it is noted that the size-independent fracture energy can be estimated either by using the load–deflection (P–δ) tail correction method (Elices *et al.*, 1992) or the boundary effect method (Guinea *et al.*, 1992), and both methods provide nearly the same size-independent fracture energy. In this study, the P–δ tail correction was adopted to compute the size-independent fracture energy. Based on the

work of Elices *et al.* (1992), Guinea *et al.* (1992) and Planas *et al.* (1992), it is known that the size dependency for the calculation of fracture energy is due to

- the testing equipment and experimental set-up
- energy dissipation in the specimen
- the non-measured energy corresponding to the unrecorded tail of the load–deflection (P–δ) curve near the end of the test.

It is also reported that curtailment of the tail of the P–δ near the end of the test results in the most significant effect on the size dependency of the measured fracture energy. This estimation of non-measured energy can be obtained by P–δ correction. Table 5 shows the size-independent fracture energy obtained for mixes R1–R5. It can be seen that there is a remarkable difference between the size-dependent and size-independent fracture energy for the same reasons as explained by Ramachandra Murthy *et al.* (2013b).

Flexural behaviour

The typical deflection hardening behaviour of UHPC of mixes R1–R5 is shown in Figure 15. The flexural behaviour of UHPC can be evaluated from several parameters. The first cracking point of UHPC is defined as the limit of proportionality (LOP) according to ASTM C1018-97 (ASTM, 1997) and the maximum equivalent bending strength point of UHPC is defined as the modulus of rupture (MOR). The LOP is the limit of the linear elastic region due to first cracking while the MOR is the point where the maximum peak load occurs. The load and deflection values at LOP and MOR are denoted P_{lop}, P_{mor}, δ_{lop} and δ_{mor} respectively. The bending strength (f_{lop}) can be calculated by using Equation 35 as given by ASTM C1609/C1609M-05 (ASTM, 2006). The energy equivalent to the area under the load–deflection curve is the toughness; the toughness T^D_{150} of a beam specimen of nominal depth D is the area under the load–deflection curve up to a net deflection of $L/150$. The equivalent flexural strength ratio $R^D_{T,150}$ is obtained using Equation 36.

$$35.\quad f_{\text{lop}} = P_{\text{lop}} \frac{L}{bh^2}$$

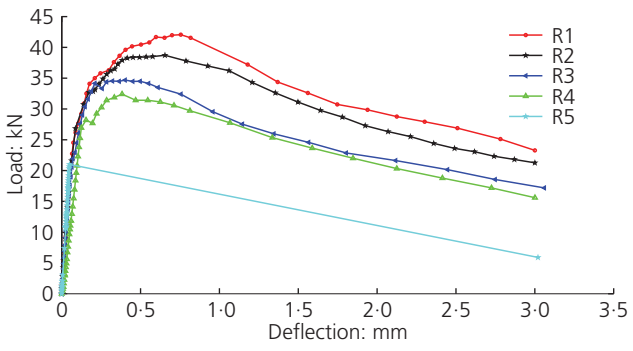

Figure 15. Load–deflection response of UHPC

$$36.\quad R^D_{T,150} = \frac{150T^D_{150}}{f_{\text{lop}}bd^2}\%$$

where L, b and h are the span, breadth and height of the prism respectively.

Besides LOP and MOR, three additional points are evaluated

- $L/600$ – net deflection equal to 1/600 of the span (0·5 mm)
- $L/150$ – net deflection equal to 1/150 of the span (2·0 mm)
- $L/100$ – net deflection equal to 1/100 of the span (3·0 mm).

ASTM C1609 (ASTM, 2006) recommends only two points, $L/600$ and $L/150$, for determining the flexural behaviour of FRC. The point $L/100$ is additionally recommended by Kim *et al.* (2011) since two points are not sufficient to describe the strain hardening of UHPC. The evaluated parameters of the tested prisms are given in Table 6, which shows that the maximum bending stress for mixes R1–R5 at MOR are 36·83, 33·95, 30·56, 28·34 and 18·84 MPa respectively.

The equivalent flexural strength ratios for mixes R1–R5 were 83·60, 85·24, 80·08, 81·30 and 0. From the results, it is very clear that flexural behaviour is enhanced due to increased RI; the maximum residual strength and toughness was found for mix R2. It may also be noticed that the deflection increases following the LOP. This result shows that the effect of fibre reinforcement is activated primarily after the LOP through fibre bridging and that the bridging forces are highly dependent upon the fibre (Naaman and El-Tawil, 2008).

The equivalent elastic bending strength values at other deflection points of interest ($L150$, $L/600$ and $L100$) are also presented in Table 6. Deflection points $L/150$ and $L/100$ are primarily intended to sample response in the softening range.

There is a need for high energy absorbing materials that will mitigate hazards for structures subjected to dynamic loads such as seismic, impact and blast loads. Thus, comparing energy absorption capacity provides useful information for such applications. The evaluated toughness of prisms R1–R4 at $L/100$ were found to be 97·21, 89·87, 76·81 and 71·00 Nm.

Conclusions

- The best curing technique for UHPC was found to be heat curing, which gave the highest compressive strength of 196 MPa at 28 d. With steam curing, only high early-age strength is attained, while the 28 d strength is less than that obtained for the case of water curing. Steam curing can thus be adopted instead of water curing if only high early-age strength is required. The 7 d strength obtained from steam curing was 120 MPa, which can be further increased by increasing the temperature and RH values. The 28 d test results obtained from XRD analysis indicate that there was

		R1	R2	R3	R4	R5
LOP	*P*: kN	27·27	32·74	22·72	26·30	—
	F: N/mm^2	23·85	28·64	19·87	23·01	—
	Deflection: mm	0·09	0·17	0·08	0·12	—
	Toughness: N.m	1·52	3·92	1·10	1·49	—
L/600	*P*: kN	40·39	38·48	34·44	31·50	—
	F: N/mm^2	35·33	33·66	30·12	27·55	—
	Deflection: mm	0·50	0·50	0·50	0·50	—
	Toughness: N.m	16·22	15·80	14·90	13·12	—
MOR	*P*: kN	42·11	38·82	34·94	32·41	21·54
	F: N/mm^2	36·83	33·95	30·56	28·34	18·84
	Deflection: mm	0·78	0·62	0·49	0·37	0·05
	Toughness: N.m	27·61	20·48	14·56	8·78	0·54
L/150	*P*: kN	29·47	26·86	22·10	21·06	—
	F: N/mm^2	25·78	23·50	19·33	18·42	—
	Deflection: mm	2·00	2·00	2·00	2·00	—
	Toughness: N.m	70·70	66·19	55·97	52·70	—
L/100	*P*: kN	23·28	21·26	17·19	15·60	—
	F: N/mm^2	20·36	18·59	15·03	13·64	—
	Deflection: mm	3·00	3·00	3·00	3·00	—
	Toughness: N.m	97·21	89·87	76·81	71·00	—

Table 6. Flexural parameters of mixes R1–R5

not much difference between water curing and steam curing in terms of the compounds formed, which explains why steam curing results only in high early-age strength and not later age strength.

- The high compressive strength obtained with heat curing could be due to the formation of a large amount of quartz in addition to portlandite and tricalcium alumino ferrite (brownmillerite). Furthermore, an increase in strength can be achieved by controlled increases in temperature and the duration of treatment. It is apparent that a high thermal regime provides the perfect situation for complete and accelerated hydration process, especially with combined mineral admixtures. By optimising the temperature and the duration of heat treatment, the hydration mechanism can be greatly varied, thus increasing the reactivity of the ingredients and leading to the superior strength gain of UHPC.
- The addition of steel fibres to UHPC increased both toughness and strain at peak stress. This behaviour is directly proportional to reinforcement index (RI), while no correlation was observed between elastic modulus and RI. The stress–strain characteristics showed that the pre-peak region has a linear ascending portion and the strain at peak stress increases with an increase in strength and RI. The post-peak curve is strongly dependent on fibre type and fibre content: it is almost as steep as the ascending curve for lower fibre contents but is more gradually sloping for higher fibre contents. The crack pattern showed the formation of vertical cracks for a lower percentage of small fibre reinforcement and diagonal cracks for higher percentages of fibre reinforcement. A stress–strain model, which can predict the complete stress–strain behaviour in both the pre-peak and post-peak regime from the RI, was formulated using the experimental data and was found to have a good correlation with the experimental data.
- Analytical models of the stress–strain relationship and toughness of UHPC in compression applicable to an RI up to 2 were proposed. The models depend on the maximum stress of the fibre concrete (considered as material strength), the corresponding strain at maximum stress, a material degradation constant β, which depends on the elastic modulus at the inflection point in the post-peak region, and the RI by volume. The experimental results were compared and analysed with models available in the literature for plain concrete, high-strength concrete, FRC and UHPC. The existing models are not able to predict the post-peak non-linearity. Hence Equations 28–32 were proposed and the results match the experimental observations satisfactorily.
- The evaluated split tensile strength, size-dependent and size-independent fracture energy, toughness, bending stress and equivalent flexural strength ratio for mixes R1–R5 were found to be in the order R1 > R2 > R3 > R4 > R5.

Acknowledgements

The paper is published with the kind permission of the Director of CSIR Structural Engineering Research Centre, Chennai. The authors acknowledge all in the Advanced Materials Laboratory who provided help and cooperation during various stages of the work.

REFERENCES

ACI (American Concrete Institute) (2008) ACI 318-08: Building code requirements for structural concrete. ACI, Farmington Hills, MI, USA.

Ambily PS, Ravisankar K, Umarani C, Dattatreya JK and Iyer NR (2013) Development of ultra-high-performance geopolymer concrete. *Magazine of Concrete Research* **66(2)**: 82–89.

Aslani F and Nejadi S (2013) Mechanical characteristics of self-compacting concrete with and without fibres. *Magazine of Concrete Research* **65(10)**: 608–622.

ASTM (American Society for Testing and Materials) (1997) ASTM C1018-97: Standard test for flexural toughness and first-crack strength of fiber reinforced concrete (using beam with third point loading). ASTM International, West Conshohoken, PA, USA.

ASTM (2006) ASTM C1609/C1609M-05: Structural test method for flexural performance of fiber reinforced concrete (using beam with third point loading). ASTM International, West Conshohocken, PA, USA, pp. 1–8.

ASTM (2014) ASTM C1240: Standard specification for silica fume used in cementitious mixtures. ASTM International, West Conshohoken, PA, USA.

Balaguru PN and Shah SP (1992) *Fiber-reinforced Cement Composites*. McGraw-Hill, New York, NY, USA.

BFUP (Bétons Fibrés à Ultra hautes Performances) AFGC (Association Française de Génie Civil) (2002) *Ultra High Performance Fibre-reinforced Concretes*: *Interim Recommendations*. AFGC/SETRA Working Group, Paris, France (in French).

Bhargava P, Sharma UK and Kaushik SK (2006) Compressive stress–strain behavior of small scale steel fibre reinforced high strength concrete cylinders. *Journal of Advanced Concrete Technology* **4(1)**: 109–121.

BIS (Bureau of Indian Standards) (1987) IS 12669.53 grade ordinary Portland cement (CED2: cement and concrete). BIS, New Delhi, India.

Carreira DJ and Chu KH (1985) Stress–strain relationship for plain concrete in compression. *ACI Journal Proceedings* **82(6)**: 797–804.

Cheyrezy M, Maret V and Frouin L (1995) Microstructural analysis of RPC (reactive powder concrete). *Cement and Concrete Research* **25(7)**: 1491–1500.

Elices M, Guinea GV and Planas J (1992) Measurement of the fracture energy using three-point bend tests: part 3 – influence of cutting the P–δ tail. *Materials and Structures* **25(6)**: 327–334.

Ezeldin AS and Balaguru PN (1992) Normal- and high-strength fiber-reinforced concrete under compression. *Journal of Materials in Civil Engineering* **4(4)**: 415–429.

Graybeal BA (2007) Compressive behavior of ultra-high-performance fiber-reinforced concrete. *ACI Materials Journal* **104(2)**: 146–152.

Graybeal BA and Hartmann JL (2003) Strength and durability of ultra-high performance concrete. *Proceedings of the 3rd International Symposium on High Performance Concrete PCI Bridge Conference, Orlando, FL, USA*, October 19–22, CD, Paper 47.

Guinea GV, Planas J and Elices M (1992) Measurement of the fracture energy using three-point bend tests: part 1 – influence of experimental procedures. *Materials and Structures* **25(4)**: 212–218.

Habel K, Viviani M, Denarié E and Brühwiler E (2006) Development of the mechanical properties of an ultra-high performance fiber reinforced concrete (UHPFRC). *Cement and Concrete Research* **36(7)**: 1362–1370.

Hillerborg A, Modéer M and Petersson PE (1976) Analysis of crack formation and crack growth in concrete by means of fracture mechanics and finite elements. *Cement and Concrete Research* **6(6)**: 773–781.

Hognestad E (1951) *Study of Combined Bending and Axial Load in Reinforced Concrete Members*. University of Illinois at Urbana Champaign, College of Engineering, Engineering Experiment Station, IL, USA.

Husem M and Gozutok S (2005) The effects of low temperature curing on the compressive strength of ordinary and high performance concrete. *Construction and Building Materials* **19(1)**: 49–53.

Karihaloo BL, Ramachandra Murthy A and Iyer NR (2013) Determination of size-independent specific fracture energy of concrete mixes by the tri-linear model. *Cement and Concrete Research* **49**: 82–88.

Kim DJ, Park SH, Ryu GS and Koh KT (2011) Comparative flexural behavior of hybrid ultra high performance fiber reinforced concrete with different macro fibers. *Construction and Building Materials* **25(11)**: 4144–4155.

Liu B, Xie Y and Li J (2005) Influence of steam curing on the compressive strength of concrete containing supplementary cementing materials. *Cement and Concrete Research* **35(5)**: 994–998.

Naaman AE and El-Tawil S (2008) Comparative flexural behavior of four fiber reinforced cementitious composites. *Cement and Concrete Composites* **30(10)**: 917–928.

Nataraja MC, Dhang N and Gupta AP (1999) Stress–strain curves for steel-fiber reinforced concrete under compression. *Cement and Concrete Composites* **21(5)**: 383–390.

Ou YC, Tsai MS, Liu KY and Chang KC (2011) Compressive behavior of steel-fiber-reinforced concrete with a high reinforcing index. *Journal of Materials in Civil Engineering* **24(2)**: 207–215.

Planas J, Elices M and Guinea GV (1992) Measurement of the fracture energy using three-point bend tests: part 2 – influence of bulk energy dissipation. *Materials and Structures* **25(5)**: 305–312.

Popovics S (1973) A numerical approach to the complete stress–strain curve of concrete. *Cement and Concrete Research* **3(5)**: 583–599.

Prem PR, Bharatkumar BH and Iyer NR (2013) Influence of curing regimes on compressive strength of ultra high performance concrete. *Sadhana* **38(6)**: 1421–1431.

Ramachandra Murthy A, Prasad BR and Iyer NR (2013a) Estimation of fracture properties for high strength and ultra high strength concrete beams and size effect. *International Journal of Damage Mechanics* **22(8)**: 1109–1126.

Ramachandra Murthy A, Karihaloo BL, Iyer NR and Raghu Prasad BK (2013b) Bilinear tension softening diagrams of concrete mixes corresponding to their size-independent specific fracture energy. *Construction and Building Materials* **47**: 1160–1166.

Ramachandra Murthy A, Karihaloo BL, Iyer NR and Raghu Prasad BK (2013c) Determination of size-independent specific fracture energy of concrete mixes by two methods. *Cement and Concrete Research* **50(19)**: 25–25.

Rilem 50-FMC (1985) Determination of the fracture energy of mortar and concrete by means of three-point bend tests on notched beams. *Materials and Structures* **18(106)**: 285–290.

Tayeh BA, Abu Bakar BH, Megat Johari MA and Voo YL (2012) Mechanical and permeability properties of the interface between normal concrete substrate and ultra high performance fiber concrete overlay. *Construction and Building Materials* **36**: 538–548.

Vandewalle L (2000) Rilem TC 162-TDF: Test and design methods for steel fibre reinforced concrete. *Materials and Structures* **33(225)**: 3–6.

Wee TH, Chin MS and Mansur MA (1996) Stress–strain relationship of high-strength concrete in compression. *Journal of Materials in Civil Engineering* **8(2)**: 70–76.

Wille K, Naaman AE, El-Tawil S and Parra-Montesinos GJ (2012) Ultra-high performance concrete and fiber reinforced concrete: achieving strength and ductility without heat curing. *Materials and Structures* **45(3)**: 309–324.

Wittmann FH, Mihashi H and Nomura N (1990) Size effect on fracture energy of concrete. *Engineering Fracture Mechanics* **35(1)**: 107–115.

Yazıcı H, Yardımcı MY, Aydın S and Karabulut AŞ (2009) Mechanical properties of reactive powder concrete containing mineral admixtures under different curing regimes. *Construction and Building Materials* **23(3)**: 1223–1231.

Yip WK (1998) Generic form of stress–strain equations for concrete. *Cement and Concrete Research* **28(4)**: 499–508.

Zheng W, Luo B and Wang Y (2014) Microstructure and mechanical properties of RPC containing PP fibres at elevated temperatures. *Magazine of Concrete Research* **66(8)**: 397–408.

Zollo RF (1997) Fiber-reinforced concrete: an overview after 30 years of development. *Cement and Concrete Composites* **19(2)**: 107–122.